

Lead Geometry and Transport Statistics in Molecular Junctions

Michael Ridley,^{1,2} Emanuel Gull,^{3,4} and Guy Cohen^{1,2, a)}

¹⁾*School of Chemistry, Tel Aviv University, Tel Aviv 69978, Israel*

²⁾*The Raymond and Beverley Sackler Center for Computational Molecular and Materials Science, Tel Aviv University, Tel Aviv 6997801, Israel*

³⁾*Department of Physics, University of Michigan, Ann Arbor, Michigan 48109, USA*

⁴⁾*Center for Computational Quantum Physics, Flatiron Institute, New York, New York 10010, USA*

We present a numerically exact study of charge transport and its fluctuations through a molecular junction driven out of equilibrium by a bias voltage, using the Inchworm quantum Monte Carlo (iQMC) method. After showing how the technique can be used to address any lead geometry, we concentrate on one dimensional chains as an example. The finite bandwidth of the leads is shown to affect transport properties in ways that cannot be fully captured by quantum master equations: in particular, we reveal an interaction-induced broadening of transport channels that is visible at all voltages, and show how fluctuations of the current are a more sensitive probe of this effect than the mean current.

I. INTRODUCTION

The conductance properties of single molecule junctions paint a rich picture of the internal dynamics of open quantum systems far from equilibrium. However, electron transport through a molecule coupled to conducting leads at finite temperature is inherently stochastic,¹ and fluctuations in the current can provide a great deal more information than the conductance or current alone.² The current, its fluctuations or noise, and higher-order statistical cumulants can be obtained from the so-called full counting statistics (FCS) approach.^{3,4} In recent years, noise and FCS techniques have been used to understand many physical properties in both experimental and theoretical transport settings. A few examples are quasiparticle charges in nanotube junctions;^{5,6} magnetic effects, channel determinations and thermotransport in atomic junctions;^{7–10} waiting time^{11,12} and first passage time¹³ distributions; correlations between currents in different leads;¹⁴ thermodynamic efficiency fluctuations;¹⁵ and fluctuation–dissipation relations.^{16–18}

The treatment of noninteracting electron transport and FCS is at an advanced stage, and both analytical and numerical methods are available.^{3,19–22} However, the inclusion of many-body interactions in even the simplest impurity models, where a small interacting impurity or molecule is coupled to large noninteracting leads, remains theoretically challenging. A variety of numerical approaches exists, each with different advantages and disadvantages depending on the particular model in question and the physical parameters. These might include, *e.g.*, a lead–molecule coupling strength Γ , a temperature $k_B T$, an applied voltage V and a local Coulomb interaction strength U .

In addition to this set of discrete energy scales, molecular conductance also depends strongly on the

geometry of the leads and the nature of the coupling between the lead and the molecule, a phenomenon which is often studied theoretically in the context of noninteracting^{23–25} and weakly correlated²⁶ systems. Transport experiments show large variation of conductance with the respect to the detailed structure of the lead–molecule interface, in particular the chemistry of the anchoring group at the interface.^{27–30} However, in simplified theoretical treatments, and especially when dealing with many-body systems, it is often convenient to neglect the internal electronic structure of the leads. One common assumption is the wide band limit approximation.^{14,31} Assuming a finite lead bandwidth D is perhaps the simplest concession to experimental reality that might be made, and is enough to show that a strong effect on transport exists even in the noninteracting case.³² A more general approach for interacting systems is therefore highly desirable.

In the regime of small lead–molecule coupling and high temperatures, the quantum master equation (QME) method offers a fast and elegant means for investigating the basic conduction properties^{33,34} and FCS^{35,36} of molecular junctions. The basic Lindblad or Redfield QME approaches assume Markovian dynamics, thus neglecting memory effects due to finite bandwidth and lead structure. Most QME methods are also perturbative in the molecule–bath coupling, and thus restricted to low-order effects like sequential tunneling. More advanced generalizations of the QME method include, for example, non-Markovian memory effects³⁷ and inelastic cotunneling processes.³⁸ Novel formulations more loosely connected to the QME even allow for the approximate treatment of strong correlations, and may also include the effects of external driving fields.^{39,40} Equation of motion approaches, also loosely related, can be formulated so as to correctly capture the noninteracting limit^{41–44}; and other approaches are exact at the semiclassical limit.^{45,46} Still, many of these approximations lack some of the advantages of more naive QME approaches, which may result, *e.g.*, in the violation of the positivity of the density matrix⁴⁷ or a

^{a)}Electronic mail: gcohen@tau.ac.il

failure to satisfy various detailed balance and fluctuation-dissipation relations.^{48,49} It is also typically difficult to verify the accuracy of these and other approximate methods or to improve them systematically.

More recent developments have lead to the emergence of approaches which map the correlated impurity model onto an auxiliary Lindblad quantum master equation where the dynamics of the impurity and a small number ($\lesssim 10$) of effective lead levels are treated at the full many-body level, with this extended system coupled to an effective Markovian environment. The auxiliary QME can then be solved using exact diagonalization (ED).^{50–52} It is possible to greatly improve this scheme by performing a perturbative expansion in the interaction that is built around the exact solution of the extended model.⁵³ Nevertheless, the many-body Hilbert space grows exponentially with the size of the extended system, and only a limited level of detail regarding the structure of the lead can therefore be included at a high level of accuracy.

There is a great deal of interest in *numerically exact* methods in this context. While this term has different definitions in the literature, here we call a method numerically exact (in some parameter regime) if arbitrarily precise results with reliable confidence intervals can be obtained at a computational scaling that is polynomial in the precision. At this level, the numerical renormalization group (NRG) method has been very successful at studying the equilibrium properties of interacting impurity models,⁵⁴ and is ideally suited for exploring low energy properties. Extensions beyond equilibrium exist and work well in many cases,^{55–58} but often struggle with large voltages, long timescales and high-energy nonequilibrium properties. Similar considerations apply to time-dependent density matrix renormalization group (tDMRG) approaches^{59–62} and multiconfiguration time-dependent Hartree-Fock.^{63–69} Promising recent advances combine some of these ideas with auxiliary master equation approaches, allowing for calculations with ~ 10 –20 auxiliary lead sites.^{70–72}

The hierarchical equation of motion (HEOM) method^{73–75} offers an alternative numerically exact scheme that is efficient for regimes in which the coupling-to-temperature ratio $\Gamma/k_B T$ is small.^{76,77} This method is different from most of the wavefunction approaches above in that it considers truly infinite leads, but relies on representing the lead density of states in terms of a sum of a small number of Lorentzian functions, making it difficult to study finite or structured bands; nevertheless, recent progress has made significant headway towards structured leads and low temperatures.^{78,79}

Another set of methods are based on iterative schemes for summing path integrals^{80–85} that allow for long time propagation and detailed leads. These methods rely on a memory cutoff that makes them difficult to converge in correlated regimes or in the presence of narrow bands or detailed structure in the leads, all of which lead to non-Markovian effects.^{86–89}

In recent years, continuous time quantum Monte Carlo (CTQMC) techniques⁹⁰ have made great progress in addressing many of the limitations mentioned above. A primary advantage is that, these being Green’s functions methods, it is straightforward to take into account an extremely large number of bath sites or even to directly take the continuum limit. Calculations involving $\sim 10^6$ lead sites or directly at the continuum limit are routinely performed, and the size or structure of the leads is not a bottleneck in practice. CTQMC is usually formulated in equilibrium and imaginary time; this is because real time implementations able to address quantum transport^{86,87,89,91–98} suffer from a dynamical sign problem. This refers to the exponential growth in the error when stochastically sampling from a number of Feynman diagrams that grows exponentially with increasing simulation time. However, the dynamical sign problem can often be effectively bypassed by an “Inchworm” algorithm (iQMC) that replaces a single simulation of the full time propagation with a series of propagation steps, each of which recycles information from previously calculated propagation steps to shorter times.^{99–104} In this regard, we note that several other interesting and promising approaches to real time quantum Monte Carlo have recently been introduced.^{105–110} In practice, obtaining numerically exact data from iQMC relies on converging the data in stochastic noise, a time discretization, and usually also a maximum diagram order. The procedures for establishing convergence, as well as the detailed scaling properties and error analysis methodologies, have been discussed at length in the literature.^{99,102,104,111}

Crucially for the present work, the computational efficiency of the iQMC approach does not directly depend on the lead structure. iQMC is therefore a promising approach to the study of quantum transport through structured molecular junctions. Furthermore, the iQMC approach was recently applied to the evaluation of FCS, allowing for preliminary studies of shot noise in the Coulomb blockade and Kondo regimes.¹³ It is therefore also possible to address noise and higher moments of the particle transport statistics in these regimes.

In this paper, we describe how iQMC can be used to study the effect of lead geometry and strong many-body interactions on the steady state current and noise characteristics of molecular junctions. We focus on the effect of the band width in a regime where the QME might be expected to perform reasonably well at the wide band limit. It is shown that while QME is able to provide us with intuition even at finite band width, its ability to provide accurate results rapidly breaks down at lower band widths. The rest of the paper proceeds as follows: Section II describes our model. In Section III A we briefly outline the iQMC approach to FCS and the calculation of cumulants within this approach. We also briefly describe the QME approach to FCS in Section III B. In Section III C we provide a practical and general numerical scheme for treating lead structure.

Two different types of leads with different dimensionality are then considered in Section IV A. The general physics from the QME viewpoint is discussed in Section IV B. The main results of the paper, showing both iQMC and QME data for the current and noise dependence on voltage for a range of different bandwidths, are presented in Section IV C. Section V contains our conclusions.

II. MODEL

We consider a real-space realization of the nonequilibrium Anderson impurity model, a simple phenomenological model of a magnetic impurity that is often used to explore transport through a molecular or atomic junction in the presence of local electron–electron interactions. The Hamiltonian is given by

$$\hat{H} = \hat{H}_M + \sum_{\ell} \hat{h}_{\ell} + \sum_{\ell} \hat{h}_{M\ell}. \quad (1)$$

Here, the isolated molecular subspace M is assumed to contain a single spin-degenerate level. It is described by the interacting local Hamiltonian

$$\hat{H}_M = \sum_{\sigma} \varepsilon^{\sigma} \hat{d}_{\sigma}^{\dagger} \hat{d}_{\sigma} + U \hat{d}_{\uparrow}^{\dagger} \hat{d}_{\uparrow} \hat{d}_{\downarrow}^{\dagger} \hat{d}_{\downarrow}, \quad (2)$$

where $\sigma \in \{\uparrow, \downarrow\}$ is a spin index and ε^{σ} is the energy needed to introduce a single electron of spin σ onto the molecule. The $\hat{d}_{\sigma}^{\dagger}$ (\hat{d}_{σ}) are creation (annihilation) operators for a spin- σ electron on the molecule, and U represents the interaction energy between two electrons simultaneously occupying the junction. The molecule is coupled to several infinite sets of noninteracting tight-binding sites comprising the leads. In particular, the term

$$\hat{h}_{\ell} = \sum_{\sigma} \sum_{i \in \ell} \varepsilon_i^{\sigma} \hat{a}_{\sigma i}^{\dagger} \hat{a}_{\sigma i} + \sum_{\sigma} \sum_{i \neq j \in \ell} t_{ij}^{\sigma} \hat{a}_{\sigma i}^{\dagger} \hat{a}_{\sigma j} \quad (3)$$

describes lead ℓ in terms of on-site energies ε_i^{σ} and hopping energies t_{ij}^{σ} . The sites i can be thought of as localized atomic orbitals. The molecule–lead coupling is given by the linear coupling term

$$\hat{h}_{M\ell} = \sum_{\sigma} \sum_{i \in \ell} \left(t_{0i}^{\sigma} \hat{a}_{\sigma 0}^{\dagger} \hat{a}_{\sigma i} + \text{H.C.} \right). \quad (4)$$

Our method is agnostic towards the specific details of the leads (*i.e.* the structure of t_{ij}^{σ} and ε_i^{σ}), but we note that we have assumed that these parameters are diagonal in spin; removing this constraint would require a generalization of the model.⁷⁶ The dynamics of physical observables in the model above when starting from a factorized initial condition can then be evaluated in terms of its dependence on the coupling density

$$\Gamma_{\ell\sigma}(\omega) = \pi \sum_{k \in \ell} |t_{0k}^{\sigma}|^2 \delta(\omega - \varepsilon_k^{\sigma}), \quad (5)$$

where the single-particle lead Hamiltonian \hat{h}_{ℓ} is diagonal in the k basis, *i.e.* $\hat{h}_{\ell} = \sum_{\sigma} \sum_k \varepsilon_k^{\sigma} \hat{a}_k^{\dagger} \hat{a}_k$. Since \hat{h}_{ℓ} is noninteracting (in the sense that it is quadratic), the diagonalization can sometimes be carried out analytically and can easily be carried out numerically for leads comprising thousands of sites. If the hopping elements t_{ij}^{σ} are local in space, it can easily be carried out numerically for millions of sites using sparse matrix techniques, and we describe how to do this below. This allows for treating a rich variety of physical systems.

III. METHODOLOGY

A. Inchworm quantum Monte Carlo

The iQMC method can be used to simulate the dynamics of a many-body quantum system prepared in some initial state and propagated in time by some Hamiltonian. The nonequilibrium steady state which forms when the system in question is open is extracted from dynamical information at the long time limit. In a coupling quench or partitioned²² approach, the system is initially in the decoupled state $\rho_0 = \rho_M \otimes \prod_{\ell} \rho_{\ell}$, a stationary state of $\hat{H}_0 \equiv \hat{H}_M + \sum_{\ell} \hat{h}_{\ell}$. At time zero, the coupling or hybridization term $\sum_{\ell} \hat{h}_{M\ell}$ is activated and particles can begin to flow between the molecule and the leads. A nonequilibrium steady state will eventually develop if the leads are chosen to be infinite and if the thermodynamic parameters (*e.g.* temperature or chemical potential) of different leads are taken to be different from each other. We assume that the molecular density matrix ρ_M is prepared in one of the four eigenstates $|\phi_i\rangle \langle \phi_i|$ of \hat{H}_M , where $\hat{H}_M |\phi_i\rangle = E_i |\phi_i\rangle$. In what follows we will focus on steady state quantities that do not depend on the choice of initial local eigenstate. Whereas most work done so far uses this partitioned method, where we propagate only along the two real-time (Keldysh) branches of the contour, it is also possible to include propagation along an imaginary time branch and introduce the voltage at the initial time. This corresponds to a voltage quench or partition-free version of the inchworm method.¹⁰² We expect the partition-free approach to be more efficient at exploring equilibrium and very small voltages, but it turns out to be more computationally expensive in the present context.

In the original iQMC approach, one evaluates the propagator

$$p_{\phi\phi'}(z_1, z_2) \equiv \langle \phi | \text{Tr}_{\{\ell\}} \left[\rho_0 T_C e^{-i \int_{z_1}^{z_2} dz \hat{H}(z)} \right] | \phi' \rangle \quad (6)$$

between two time points z_1, z_2 on the Keldysh contour, where ϕ and ϕ' denote different atomic states for the initial preparation and T_C is the contour time-ordering operator. This is done by expanding $p_{\phi\phi'}$ in powers

of the hybridization and summing the resulting diagrammatic series stochastically. Modified propagators describing specific observables are also evaluated.⁹⁷ Instead of summing over all possible diagrams on the contour in what constitutes a brute force or “bare” Monte Carlo approach,⁹³ the iQMC algorithm incrementally evaluates propagators on longer and longer time intervals along the contour, while optimally reusing propagator data computed on shorter intervals. This avoids the dynamical sign problem in a wide variety of cases, and the scaling of the computational cost with simulation time is effectively reduced from exponential to quadratic.⁹⁹ In practice, we typically limit an additional diagram order parameter approximately corresponding to the maximum order of the self-energy in a self-consistent diagrammatic expansion; the method becomes inefficient if the order needed to obtain convergence is very large,¹⁰⁴ which we expect to happen when the underlying expansion does not capture the physics of the parameter regime under investigation.¹⁰¹

Recently, the iQMC technique was extended to the study of FCS of particle transport.¹³ Rather than evaluating the propagator in Eq. 6, we evaluate the moment generating function for some lead ℓ ,

$$Z_\ell(\lambda, t) \equiv \sum_{\Delta n_\ell} P(\Delta n_\ell, t) e^{i\lambda \Delta n_\ell}. \quad (7)$$

Here, $P(\Delta n_\ell, t)$ is the probability that the number of particles in lead ℓ has changed by Δn_ℓ at time t . The expression for $Z(\lambda, t)$ can be reformulated as a propagator $p_{\phi\phi'}^\lambda$ in which the Hamiltonian is modified by a counting field λ .^{2,13,21} The parameter λ changes sign as the time variable crosses the folding point on the Keldysh contour and the subsequent modification to the Hamiltonian only affects the hybridization term, $\hat{h}_{M\ell}(z) \rightarrow \hat{h}_{M\ell}(\lambda; z)$.^{13,21}

The technical details regarding the iQMC algorithm and the evaluation of $Z(\lambda, t)$ including all modifications to the iQMC algorithm are discussed at length elsewhere.^{13,99,102} For the purposes of the present work we merely note that the k^{th} order statistical cumulant is extracted from k^{th} order logarithmic derivative of $Z_\ell(\lambda, t)$ with respect to λ :

$$C_{\ell,k}(t) = \frac{\partial^k \log(Z_\ell(\lambda, t))}{\partial (i\lambda)^k}. \quad (8)$$

The steady state current and current noise in lead ℓ are then evaluated from the asymptotic gradients of the first and second order cumulants:

$$I_\ell = \lim_{t \rightarrow \infty} \frac{C_{1,\ell}(t)}{t}, \quad (9)$$

$$S_\ell = \lim_{t \rightarrow \infty} \frac{C_{2,\ell}(t)}{t}. \quad (10)$$

In iQMC, since the logarithmic derivatives are performed numerically over noisy data, the extraction of specific cumulants becomes increasingly difficult as their order grows.

B. Master equations

In this section, we briefly outline the Markovian QME treatment that we use to compare with the iQMC method and as a guide to our exploration of the parameter space. The QME provides an approximate expression for the dynamics of the reduced density matrix describing the embedded molecule, $\hat{\sigma}(t) \equiv \text{Tr}_{\{\ell\}} \{\hat{\rho}(t)\}$. Here ℓ is the lead subspace, and $\hat{\sigma}$ is therefore a 4×4 matrix in the many-body molecular basis $|\phi_i\rangle$. Since the local Hamiltonian and the hybridization are diagonal in this basis, the different site populations are not coupled through the off-diagonal terms of $\hat{\sigma}(t)$ and we may neglect coherences. We thus write down a simple equation of motion for the four diagonal matrix elements $p_i = \langle \phi_i | \hat{\sigma}(t) | \phi_i \rangle$:

$$\frac{dp_i(t)}{dt} = \sum_j M_{ij} p_j(t). \quad (11)$$

The matrix elements $M_{ij} \equiv \langle \phi_i | \hat{M} | \phi_j \rangle = \sum_\ell M_{ij}^\ell$ correspond to transition rates from dot state j to state i as mediated by the lead ℓ :

$$M_{ij}^\ell = \begin{cases} -\sum_k R_{ki}^\ell & i = j, \\ R_{ij}^\ell & i \neq j. \end{cases} \quad (12)$$

Here, the rates R_{ij}^ℓ are given by

$$R_{ij}^\ell = |\epsilon_{ij}| \Gamma_\ell(\epsilon_{ij} \Delta E_{ij}) f_\ell(\Delta E_{ij}). \quad (13)$$

These rates therefore depend on the coupling density $\Gamma_\ell(\omega)$ and the Fermi function $f_\ell(\omega) = (e^{\beta(\omega - \mu_\ell)} + 1)^{-1}$, as well as on the energy differences between molecular states $\Delta E_{ij} \equiv E_i - E_j$. We also use the definition and $\epsilon_{ij} = \pm 1$ for $n_i - n_j = \pm 1$ and $\epsilon_{ij} = 0$ otherwise, where n_i is the number of electrons on the molecule in the local state $|\phi_i\rangle$; and the fact that $f_\ell(-\Delta E) = 1 - f_\ell(\Delta E)$. Intuitively, the rate R_{ij}^ℓ for $\epsilon_{ij} = 1$ describes a process where the molecule goes from state j to state i by absorbing an electron of energy ΔE_{ij} from an occupied level in the leads, and the corresponding rate for $\epsilon_{ij} = -1$ describes a process where an electron of energy $\Delta E_{ji} = -\Delta E_{ij}$ is released into the leads.

In the presence of a nonzero counting field λ , the modified populations $p_i(t) \rightarrow p_i(\lambda, t)$ are obtained by modifying the matrix elements in Eq. 12 according to

$$M_{ij}^\ell \rightarrow M_{ij}^\ell e^{i\lambda \epsilon_{ij}}. \quad (14)$$

The generating function $Z(\lambda, t)$ is then obtained as the trace with respect to the molecular subsystem,^{2,35,112}

$$Z(\lambda, t) = \text{Tr}_S [\hat{\sigma}(\lambda, t)] = \sum_i p_i(\lambda, t), \quad (15)$$

and all cumulants can be extracted as described in Section III A.

C. Coupling density

For completeness, we will briefly review how the coupling density Eq. 5 for a particular lead is obtained in practice, given a concrete model of the system and leads. To simplify the discussion and the notation we will drop the ℓ and σ subscripts. We further assume (as is the case in the rest of this work) that the molecule is coupled only to a single site in the lead, such that

$$t_{0i} = \delta_{i1} t_M. \quad (16)$$

It is straightforward to generalize this to more complex models than that used here; for example, analogous procedures for time-dependent noninteracting transport and in the presence of secondary Markovian leads have been discussed in detail in the literature.^{25,113–116}

We begin by rewriting Eq. 5 in terms of Green's functions:

$$\Gamma(\omega) = \pi \sum_k |t_{0k}|^2 \delta(\omega - \varepsilon_k) = \frac{1}{2} \sum_k |t_{0k}|^2 A_k(\omega), \quad (17)$$

where $A_k(\omega)$ is the spectral function of the noninteracting lead in the diagonal k basis. This is given by the imaginary part of the retarded Green's function $G_k^R(\omega)$:

$$\begin{aligned} A_k(\omega) &= -2\Im \{G_k^R(\omega)\}, \\ G_{ij}^R(\omega) &= \mathcal{F} \{G_{ij}^R(t)\}, \\ G_{ij}^R(t) &= i\vartheta(t) \left\langle \left[\hat{a}_i^\dagger(0), \hat{a}_j(t) \right] \right\rangle. \end{aligned} \quad (18)$$

Here, \mathcal{F} is a Fourier transform from time to frequency and $\vartheta(t)$ is the Heaviside step function. The diagonalization of the lead subspace \hat{h} (corresponding to a single spin component of \hat{h}_ℓ above) is performed in the single particle picture, *i.e.*

$$\varepsilon_k = \sum_{ij} V_{ki} \langle i | \hat{h} | j \rangle V_{jk}^\dagger, \quad (19)$$

with V_{ki} a unitary matrix whose dimension is the number of sites in the lead, which we will denote as N . The states $|i\rangle = \hat{a}_i^\dagger |0\rangle$ are obtained by adding a single electron to the vacuum state $|0\rangle$. The matrix $V_{ki} = \langle k | i \rangle$ defines the diagonal k basis and its relationship to the real space i, j basis. In particular, it allows us to make

the transformations

$$\begin{aligned} A_k(\omega) &= \sum_{ij} V_{ki} A_{ij}(\omega) V_{jk}^\dagger, \\ |t_{0k}|^2 &= t_{k0} t_{0k} = \sum_{ij} V_{ki} t_{i0} t_{0j} V_{jk}^\dagger = |t_M^2| V_{k1} V_{1k}^\dagger. \end{aligned} \quad (20)$$

In the last equality, we have used Eq. 16. Plugging Eq. 20 into Eq. 17 we obtain

$$\begin{aligned} \Gamma(\omega) &= \frac{|t_M^2|}{2} \sum_k V_{k1} A_k(\omega) V_{1k}^\dagger \\ &= \pi t_M^2 A_{11}(\omega). \end{aligned} \quad (21)$$

Our task is therefore reduced to calculating the local spectral function at a single site on the lead.

While this task might most intuitively be carried out simply by diagonalizing $\langle i | \hat{h} | j \rangle$, one is often interested in large leads. Unless the diagonalization can be carried out analytically, numerical diagonalization of the $N \times N$ matrix is needed. The computational time for this scales as $O(N^3)$ and the memory as $O(N^2)$. However, given short-ranged hopping terms, the matrix $\langle i | \hat{h} | j \rangle$ is very sparse and therefore the diagonalization can benefit from sparse matrix techniques, which reduce both the time and memory costs to $O(N)$. Such techniques are well known in the quantum transport literature and implemented in widely used packages such as Kwant.¹¹⁷ A particularly simple and useful approach is based on the so-called kernel polynomial method,¹¹⁸ and we briefly outline it here.

We rewrite Eq. 21 as

$$\begin{aligned} \Gamma(\omega) &= \frac{|t_M^2|}{2} \sum_k \langle k | 1 \rangle A_k(\omega) \langle 1 | k \rangle \\ &= \pi |t_M^2| \sum_k |\langle 1 | k \rangle|^2 \delta(\omega - \varepsilon_k). \end{aligned} \quad (22)$$

Let us assume that we are working in a set of units such that $\Gamma(\omega)$ is nonzero only within a range of frequencies $-1 < \omega < 1$. For any physical lead with a finite bandwidth, this constraint can be enforced by finding the highest and lowest eigenvalue of \hat{h} , for example with the Lanczos method, and then appropriately rescaling \hat{h} . Given this, we can expand $\Gamma(\omega)$ in a series of Chebyshev polynomials $T_n(\omega)$:

$$\begin{aligned} \Gamma(\omega) &= \frac{1}{\pi \sqrt{1-x^2}} \left[\mu_0 + 2 \sum_{n=1}^{\infty} \mu_n T_n(\omega) \right], \\ \mu_n &= \int_{-1}^1 \Gamma(\omega) T_n(\omega) d\omega. \end{aligned} \quad (23)$$

Combining Eq. 22 and Eq. 23 gives

$$\begin{aligned}\mu_n &= \pi |t_M^2| \sum_k |\langle 1|k\rangle|^2 T_n(\varepsilon_k) \\ &= \pi |t_M^2| \sum_k \langle 1|T_n(\hat{h})|k\rangle \langle k|1\rangle \\ &= \pi |t_M^2| \langle 1|T_n(\hat{h})|1\rangle.\end{aligned}\quad (24)$$

The n^{th} moment is therefore given in terms of the action of the n^{th} Chebyshev polynomial of the Hamiltonian \hat{h} on the state $|1\rangle$:

$$\begin{aligned}\mu_n &= \pi |t_M^2| \langle 1|\alpha_n\rangle, \\ |\alpha_n\rangle &= T_n(\hat{h})|1\rangle.\end{aligned}\quad (25)$$

Now, using the recurrence relations connecting the Chebyshev polynomials, it is easy to show that

$$\begin{aligned}|\alpha_0\rangle &= |1\rangle, \\ |\alpha_1\rangle &= \hat{h}|1\rangle, \\ |\alpha_{n+1}\rangle &= 2\hat{h}|\alpha_n\rangle - |\alpha_{n-1}\rangle.\end{aligned}\quad (26)$$

To obtain coefficients up to any finite n it is therefore necessary only to multiply a sequence of vectors in the single particle $|i\rangle$ basis by the sparse matrix \hat{h} , a numerical task which can be accomplished in $O(N)$ steps, and apply Eq. 26 recursively. The expansion is stable, inexpensive to perform and converges rapidly. In practice, it is usually numerically beneficial to convolve the results by a kernel; for this particular case, a Lorentz kernel with a small width parameter λ should be used to maintain causality. Standard techniques allow this to be done by modifying the expansion coefficients such that $\mu_n \rightarrow g_n \mu_n$, where $g_n = \frac{\sinh(\lambda(1-\frac{n}{N}))}{\sinh(\lambda)}$.¹¹⁸

IV. RESULTS

A. Lead geometry, coupling density and bandwidth

It is common and convenient in the study of molecular electronics and other quantum transport problems to assume the wide band limit,

$$\Gamma_{\ell\sigma}^{\text{wideband}}(\omega) \simeq \Gamma_{\ell\sigma} = \text{const.} \quad (27)$$

We will begin by briefly considering how and when this limit emerges in nanoscale electronics. In Fig. 1, we consider two simple cases of molecular (or possibly atomic) junctions with two leads, $\ell \in \{L, R\}$. In the top part of the figure, each lead is a one-dimensional chain of identical s -orbital sites with nearest-neighbor couplings, such that $\varepsilon_i^\sigma = \varepsilon_{b\ell}$, $t_{ij}^\sigma = t_b \delta_{i,j\pm 1}$ and $t_{0i}^\sigma = \delta_{i1_\ell} t_M$, where 1_ℓ is the index of the site in lead ℓ adjacent to the molecule (this is the Anderson-Newns model¹¹⁹). At the limit of

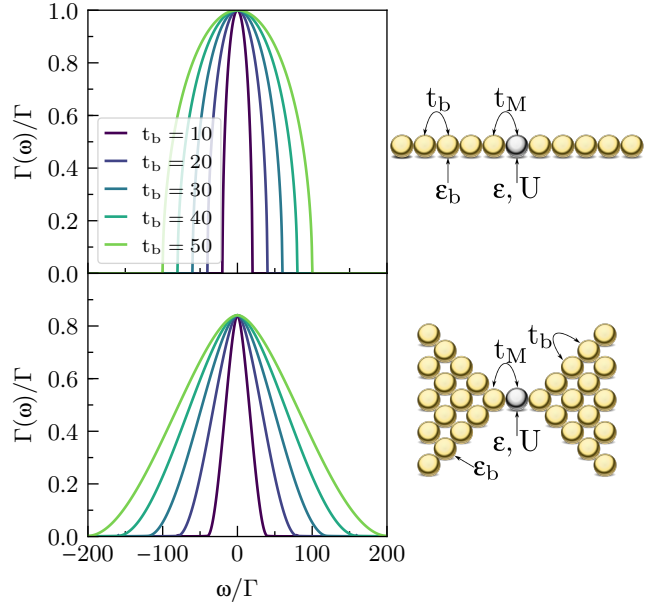


Figure 1. The coupling density $\Gamma_{\ell\sigma}(\omega) = \Gamma(\omega)$ for a single lead $\ell \in \{L, R\}$ and spin σ is shown in the left panels for several values of t_b , given two different types of leads illustrated in the right panels. On top, a one-dimensional chain is considered (with scaling $t_M = \sqrt{t_b}\Gamma$). On the bottom, a two-dimensional square lattice coupled to the molecule at its corner is shown (with scaling $t_M = t_b$).

an infinitely long chain, $\Gamma(\omega)$ can be evaluated analytically and forms an ellipse:

$$\Gamma_{\ell\sigma}^{1D}(\omega) = \begin{cases} \frac{t_M^2}{2t_b^2} \sqrt{4t_b^2 - (\omega - \varepsilon_{b\ell})^2} & |\omega - \varepsilon_{b\ell}| \leq 2t_b, \\ 0 & \text{otherwise.} \end{cases} \quad (28)$$

The value of t_b sets the bandwidth $D = 4t_b$, and the function $\Gamma(\omega)$ attains its maximum value of $\frac{t_M^2}{t_b}$ when $\omega = \varepsilon_{b\ell}$. To simplify our exploration of the parameter space, we set $\frac{t_M^2}{t_b} \equiv \Gamma$ to hold this maximum value constant and use Γ as our standard unit of energy; we therefore have $t_M = \sqrt{t_b}\Gamma$. The result is plotted for a series of values of t_b with $\varepsilon_{b\ell} \equiv \varepsilon_b = 0$ in the top left panel of Fig. 1. The same parameters will be used throughout most of the following sections. To minimize the notation, we also set $\hbar = e = 1$, such that all units are given in terms of Γ . In addition, we choose to perform calculations in the left lead, so that simplified notations for current ($I \equiv I_L$) and noise ($S \equiv S_L$) may be chosen.

It is clear that the wide band limit emerges when t_b is significantly larger than all other energy scales. It is not clear that this limit should be generally applicable within molecular electronics. Importantly, in the presence of strong local interactions U or large potential differences between the leads, the curvature at small frequencies in Fig. 1 suggests that significant deviations from the wide band limit can be expected to occur even when t_b is 50 times the magnitude of the maximal dot-bath coupling. This result does not strongly

depend on our choice of parameter scaling. The bandwidth, on the other hand, should be a dominant factor only for smaller values of t_b .

In more concrete terms, our parameters range from the case where hopping energies (or nearest-neighbor overlaps between orbitals at adjacent atoms) within the metallic leads, t_b , are $\sqrt{10} \sim 3.16$ times larger than the molecule-lead hopping t_M ; to the case where t_b is $\sqrt{50} \sim 7.07$ times larger than t_M . Such parameters could conceivably be realized in either molecular electronics junctions or atomic junctions under strain. For much weaker molecule-lead coupling, the wide band limit becomes appropriate and master equations may be expected to perform well at high temperatures. When $t_b \sim t_M$, it is immediately clear from the considerations above that master equations should not be applied at any temperature, and we will not address this regime here.

The one-dimensional case is extreme, and it would be prudent to take into account the role of lead dimensionality. In the bottom part of Fig. 1 we therefore consider a semi-infinite two-dimensional square lattice with its corner coupled to the molecule. Here, $\varepsilon_i^\sigma = \varepsilon_{b\ell}$, $t_{ij}^\sigma = t_b \delta_{i,j \in \text{n.n.}}$ and $t_{0i}^\sigma = t_M \delta_{i1_\ell}$ where the site $i = 1_\ell$ is at the corner of the lattice, adjacent to the molecule. While the particular coupling density in this case may perhaps be obtainable analytically (as are the one-dimensional case above and, incidentally, the infinite-dimensional hypercube where a Gaussian is obtained¹²⁰), we solve for it numerically using the more general kernel polynomial scheme outlined in section III C. One immediate difference with respect to the one-dimensional case is in the scaling needed to maintain a constant maximum value of $\Gamma(\omega)$: here we take $t_M = t_b$. A second difference is in the bandwidth, which is $D = 8t_b$ instead of $4t_b$. Finally, the cutoff at the band edge occurs much more smoothly in this case.

We reiterate that our iQMC method is compatible with any $\Gamma_{\ell\sigma}(\omega)$, corresponding to any particular lead geometry, as an initial input. Here, we will proceed to examine the one-dimensional Anderson-Newns chain within both the QME and iQMC methods, focusing on the effect of the finite bandwidth. Interacting calculations for the 2D square corner geometry and other higher-dimensional cases will not be presented here.

B. General picture within master equations

Having established the general behavior of the coupling density within the model, we continue to explore its effect on transport properties. It is useful to start from an overall view connecting well-known Coulomb blockade physics at the wide band limit (corresponding to a large value of the hopping within the leads, t_b) with the behavior at small band width (corresponding to small t_b). Furthermore, we will consider parameters where Γ is 1–2 orders of magnitude smaller than every energy scale in the Hamiltonian, and the

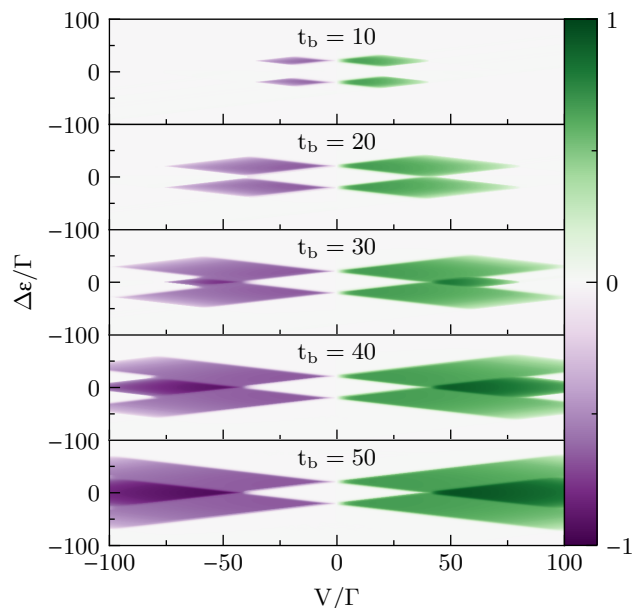


Figure 2. The master equation approximation to the steady state current I in the chain is plotted as a function of the bias voltage $V = \mu_L - \mu_R$ and the gate voltage $\Delta\varepsilon$. The different panels show $I(V, \Delta\varepsilon)$ at several values of the lead hopping energy t_b , which determines the bandwidth $D = 4t_b$. The interaction strength is $U = 40\Gamma$, the molecular level is at $\varepsilon_M = -\frac{U}{2} + \Delta\varepsilon$ and the temperature is $k_B T = \Gamma$.

temperature $k_B T$ is much larger than the Kondo temperature, at which strongly correlated physics becomes important. At such parameters, it is widely assumed in the literature that master equations can provide us with at least a qualitatively correct picture. Specifically, we choose interaction strength $U = 40\Gamma$ and temperature $k_B T = \Gamma$, far from the correlated regime; and apply bias voltages V such that the chemical potentials in the leads are $\mu_\ell = \varepsilon_{b\ell} = \frac{V}{2}$ for $\ell = L$ and $\mu_\ell = \varepsilon_{b\ell} = -\frac{V}{2}$ for $\ell = R$. We also set the energy of half-filled states to $\varepsilon = -\frac{U}{2} + \Delta\varepsilon$, such that the particle-hole symmetric point is found at $\Delta\varepsilon = 0$. Experimentally, $\Delta\varepsilon$ corresponds to a shift in the molecular potential or gate voltage caused by electrostatic coupling to a third electrode.¹²¹ In a typical experiment a sweep of both the bias and gate voltages is performed so that so-called stability diagrams can be constructed showing contour plots of transport quantities as a function of both parameters.¹²²

In Fig. 2 we plot the steady state current I within the master equation approximation as a function of the bias and gate voltages, V and $\Delta\varepsilon$, at the same series of t_b values considered in Fig. 1. At small t_b (upper panel), the current is strongly suppressed throughout the figure, whereas at large t_b (lower panel) the familiar Coulomb blockade diamond structure from the wide band limit¹²¹ is gradually restored.

The wide band picture, most closely approximated by the lowest panel of Fig. 2, is characterized by—at in-

creasing voltage—regions with no current; regions with where some of the conduction channels are open, and the current plateaus at $I = \frac{2}{3}\Gamma$; and regions where all channels are open, and the current plateaus at $I = \Gamma$.¹²³ As the bandwidth decreases (in increasingly higher panels) Finite bandwidth resulting from the one-dimensional leads suppresses high voltage transport in all channels, since no lead levels are available to transfer electrons at higher energies. The small bandwidth more strongly suppresses the opening of the second set of channels, which are associated with higher energy transport processes. Therefore, the dark triangles completely disappear at $t_b \lesssim 20\Gamma$ and are smaller at $t_b \sim 30\Gamma$. In particular, there exists a region within the $t_b = 30\Gamma$ plot (central panel) where at voltages $V \simeq 50\Gamma$ full and partial transport are separated in $\Delta\varepsilon$ by a zero transport region. At slightly higher voltages, full transport is completely suppressed whereas partial transport (at certain values of $\Delta\varepsilon$) remains possible.

We note that it is possible to repeat this calculation with either QME or iQMC for the two-dimensional leads (or any other leads), and obtain results which differ quantitatively, since both the shape and the width of the band will differ. However, as we are chiefly interested in the qualitative effect of the limited bandwidth in the present scope, we will continue to consider only the one-dimensional case.

It is now natural to ask whether the theoretical analysis above is accurate. Temperature plays a central role here. Within the QME approximation, the main effect of temperature is to smear out the borders between the different conduction regions. At higher temperatures these borders become smoother, and at lower temperatures they become sharper. It is well understood that at very low temperatures the QME breaks down, and that transport within the Kondo and mixed valence regimes is dominated by entirely different mechanisms than those addressable by the QME. However, at the parameters of Fig. 2 the system is almost three orders of magnitude above the Kondo temperature,¹²⁴ and strong correlation effects should be largely irrelevant. Nevertheless, the interaction is large enough that one might question the accuracy of the single-particle picture in the leads after the activation of the coupling. It is therefore of some interest to examine an exact numerical solution of the model.

We emphasize that iQMC, the numerically exact method we will use, is not restricted to high temperatures or weakly correlated physics. In fact, in much of the work so far, iQMC has been used to study the strongly correlated Kondo regime.^{13,53,99,102,103} We limit ourselves to high temperatures specifically so that any breakdown of QME is unrelated to Kondo and therefore due only to the finite nature of the band.

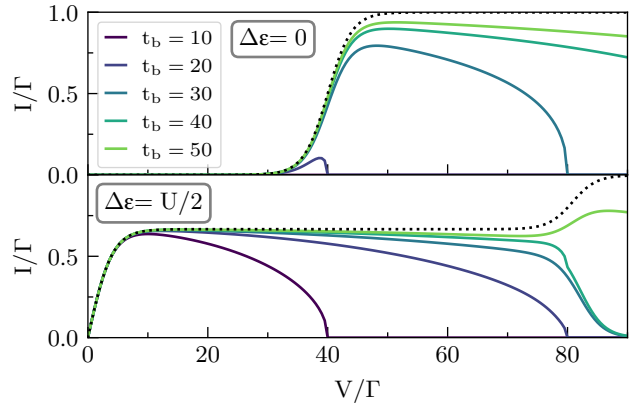


Figure 3. The master equation approximation to the steady state current I in the chain is shown as a function of bias voltage V , for gate voltages at the symmetric point $\Delta\varepsilon = 0$ (top) and at $\Delta\varepsilon = \frac{U}{2}$ (bottom). The different curves in each panel show several values of the lead hopping energy t_b , which determines the bandwidth $D = 4t_b$. The interaction strength is $U = 40\Gamma$, the molecular level is at $\varepsilon_M = -\frac{U}{2} + \Delta\varepsilon$ and the temperature is chosen such that $k_B T = \Gamma$. As a guide to the eye, the dotted curves in the two panels are the corresponding master equation result at the wide band limit.

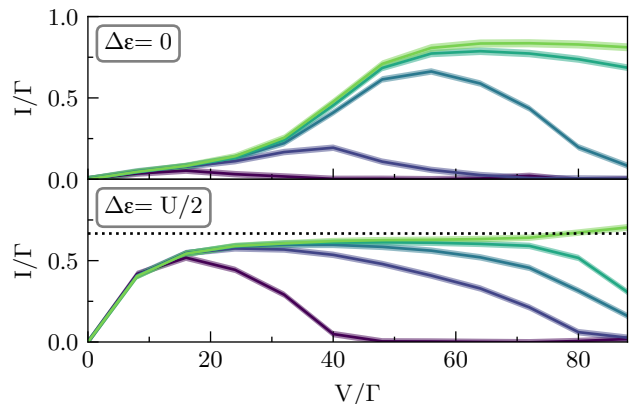


Figure 4. The numerically exact steady state current I in the chain obtained from iQMC is shown as a function of bias voltage V , for gate voltages at the symmetric point $\Delta\varepsilon = 0$ (top) and at $\Delta\varepsilon = \frac{U}{2}$ (bottom). Parameters are as in Fig. 3.

C. Master equations vs. numerically exact iQMC results

We now present our main results: an exploration of the phenomena predicted by the master equation approximation in section IV B within iQMC. In addition to the current I , we will also present data for the shot noise S . To this end, we simulate the dynamics of the generating function $Z(\lambda, t)$ up to a finite time t and for a constant value of λ , as described in Sec. III A. For the results shown here, since we are far from the strongly correlated regime, to obtain reasonably reliable results it is sufficient to go to time $t = \frac{2}{\Gamma}$ and to limit the maximum order of Inchworm diagrams to 3, corresponding to a 2-crossing approximation. For some of the more difficult

parameters, we verified convergence by considering both longer times and higher maximum orders (not shown). This is in contrast with the strongly correlated regime of this model, where it is often necessary to propagate to substantially longer times and orders.^{53,99,104,125} Kondo physics can also result in very slow spin dynamics requiring access to longer time scales,^{13,89,99} but this is not relevant here. At each point on our plots, we display an average of the asymptotic value of $I(V)$ and $I(-V)$ from two independent runs as our current I , and $\Delta I \equiv |I(V) - I(-V)|$ as a rough error estimate combining finite-time errors with stochastic errors. In the error bars below, we bound the error estimates from below by 3% for the current and 5% for the noise; and also by absolute values of 0.01Γ and $0.01\Gamma^2$, respectively.

A preliminary value for any data point shown below can be obtained within minutes on a small cluster, whereas accurate high resolution benchmarks can be obtained in hours. Here, we take a middle path between these extremes by attempting to keep all relative errors for the current within a range of $\sim 3\%$. Since the calculations remain rather expensive, we forgo the two-dimensional contour plot and concentrate on the two arguably most interesting cuts through Fig. 2: the symmetric point at $\Delta\varepsilon = 0$ and the point at which current is maximized at small voltages, $\Delta\varepsilon = \frac{U}{2}$. This second point is also the tip of the lighter parallelogram shaped regions that signify partial transport. Due to the same cost, Fig. 4 and Fig. 6 are plotted on a rougher voltage grid than Fig. 3 and Fig. 5.

In Fig. 3 we display these two cuts across the data, still within the master equations. The two panels (top and bottom) show the two values of $\Delta\varepsilon$ ($\Delta\varepsilon = 0$ and $\Delta\varepsilon = \frac{U}{2}$, respectively). All values of t_b are plotted simultaneously, making it easier to identify some of the main features. Before we point these out, we suggest that the reader examine and compare the figure with Fig. 4, which shows the corresponding iQMC data. A cursory glance reveals both similarities and differences, meriting a discussion of the features that takes both sets of results into account.

At large bandwidths ($t_b = 50\Gamma$), it is clear that master equations provide an adequate physical picture, especially at large voltages. The main difference in going from the QME to the iQMC picture is a broadening of features in the $I(V)$ curves. At smaller bandwidths, where the Markovian approximation may be expected to lose its accuracy, the differences become increasingly dramatic. The sharp cutoff of current at the points where the bias voltage shifts the lead bands out of resonance with each other is softened, especially at the symmetric point $\Delta\varepsilon = 0$. Whereas the master equations predict essentially no current at any voltage at the symmetric point for $t_b = 10\Gamma$, the exact result shows that the current is clearly distinguishable from zero at voltages $V \lesssim U$. For $t_b = 20\Gamma$, master equations predict nonzero current over only a small voltage region near $V \approx U$, while the exact calculation reveals currents for a wide range of voltages $0 < V \lesssim 2U$. While the master

equations predict a broad and robust region of negative differential conductance at $\Delta\varepsilon = \frac{U}{2}$ at any finite bandwidth, the exact results shift the beginning of this region to increasingly higher voltages as t_b increases, such that it eventually disappears completely in the voltage range shown.

Despite all these differences, it is interesting to note that the suppression of transport in the regime where all channels are open at the wide band limit, as predicted by master equations, is reproduced in the exact results—though to a lesser degree. This tells us that while master equations may not provide us with a quantitative picture of currents at this physical regime, they are still capable of providing some insight into the relevant transport mechanisms. For example, the language of discrete transport channels, though approximate, remains useful.

The qualitative differences between the QME and iQMC data are due to many-body correlation effects between the molecule and the leads. Such effects are not accounted in the QME approximation. The broadening observed here (at both large and small bandwidths) is different from broadening due to the molecule-lead coupling, which is also not present in master equations; that effect is of order Γ , whereas the broadening observed here is more commensurate with the size of the interaction strength $U = 40\Gamma$. Since U is rather large here (and was chosen this way because all energy scales must be much larger than Γ for master equations to be valid), a low-order perturbative expansion in the many-body interaction cannot quantitatively capture this effect.

Next, we discuss shot noise. In Fig. 5 we show the master equation approximation, while in Fig. 6 we present the corresponding iQMC data. Although the statistical errors associated with the noise are greater than those for the current, as discussed in Section. III A, the noise is a more sensitive probe of the available transport channels than the current. This has several interesting implications for the correlated dynamics that can be clearly seen in the data.

Current fluctuations can occur in conductors held at finite temperature even without a bias voltage. The source of these fluctuations lies in the thermal agitation of conducting electrons, and is referred to as the thermal noise or Johnson–Nyquist noise. In Fig. 5 and Fig. 6, at the leftmost point $V = 0$, the Johnson–Nyquist noise is shown at the particle–hole symmetric gate voltage $\Delta\varepsilon = 0$ (top) and at $\Delta\varepsilon = \frac{U}{2}$ (bottom). Within QME (Fig. 5) the thermal noise is zero at the symmetric point, but takes on a finite value at $\Delta\varepsilon = \frac{U}{2}$. However, the iQMC data (Fig. 6) indicates the existence of a finite thermal noise at both gate voltages. In particular, the thermal noise at the symmetric point is comparable in magnitude to the finite voltage shot noise, and appears to be weakly enhanced for larger values of t_b .

The noise also remains a more sensitive probe of many-body scattering effects than the current at higher bias voltages V . In particular, the iQMC noise (Fig. 6) shows a more significant broadening than that in the

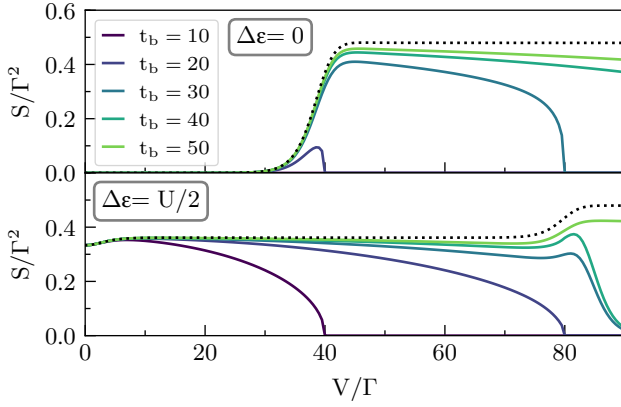


Figure 5. The master equation approximation to the steady state shot noise S in the chain is shown as a function of bias voltage V , for gate voltages at the symmetric point $\Delta\epsilon = 0$ (top) and at $\Delta\epsilon = \frac{U}{2}$ (bottom). Parameters are as in Fig. 3.

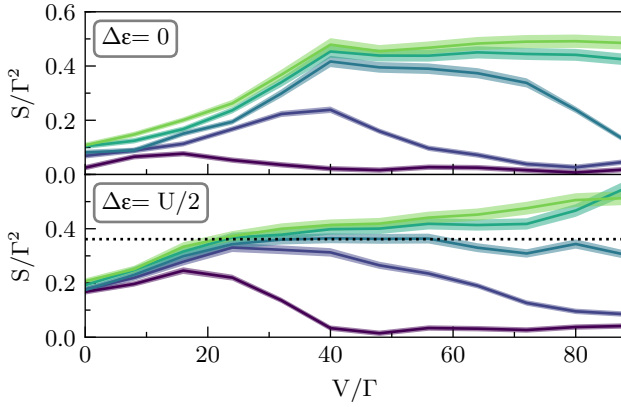


Figure 6. The numerically exact steady state shot noise S in the chain obtained from iQMC is shown as a function of bias voltage V , for gate voltages at the symmetric point $\Delta\epsilon = 0$ (top) and at $\Delta\epsilon = \frac{U}{2}$ (bottom). Parameters are as in Fig. 5.

current plots of Fig. 4. Another striking difference is that the iQMC noise rapidly exceeds the QME plateaus, clearly indicating an opening of the higher energy channels at lower voltage that was not visible in the current. At the lower bandwidths and high bias, where iQMC predicts no current, nonzero current fluctuations clearly remain. This suggests that some transport channels are not yet fully closed, but nevertheless carry no current on average.

V. CONCLUSIONS

The electronic structure of the leads plays an essential role in dictating the conductance properties of molecular junctions, which is lost when one only considers the wide band limit, where Markovian QME approximations are appropriate. We presented a numerically exact study of nonequilibrium transport in the Anderson-Newns model, which describes an interacting im-

purity coupled to a one dimensional chain, using the numerically exact iQMC method. Our methodology provides not only the expectation value of the current, but also the full counting statistics of particle transport, and can easily be extended to any lead geometry. We have provided a detailed discussion of how this can be done numerically for very large leads with potentially complex structure, and discussed the effect on the band width and shape when the leads are modified from the one dimensional chain structure to a two dimensional square lattice. We leave study of the interacting square lattice, and the effect of dimensionality in general, to future work.

We found that the finite bandwidth of the chain can suppress high energy transport channels. Whereas the QME approximation predicts the clean closure of transport channels above some threshold voltage set by the bandwidth, the iQMC method shows that transport continues to exist at a larger range of voltages. Our results suggest that this is facilitated by an interaction-induced “smearing” of transport characteristics that partially opens conduction channels forbidden within the QME approximation, and also allows transport at lower voltages.

Our results further show an enhancement of the thermal noise compared to QME. This enhancement depends only weakly on the lead bandwidth. At certain parts of the parameter space we explored, the mean current is entirely suppressed by the bandwidth, but its fluctuations are not. This suggests that some transport processes are not forbidden, but only average to zero, and is a powerful demonstration of Landauer’s maxim that “the noise is the signal” in molecular electronics.¹²⁶ Understanding this effect and how it might be manipulated is a promising direction for future work.

Acknowledgments G.C. acknowledges support by the Israel Science Foundation (Grant No. 1604/16). M.R. was supported by the Raymond and Beverly Sackler Center for Computational Molecular and Materials Science, Tel Aviv University. E.G. was funded by DOE Grant No. ER 46932. This collaboration was supported by Grant No. 2016087 from the United States-Israel Bi-national Science Foundation (BSF).

REFERENCES

- ¹Y. M. Blanter and M. Büttiker, *Physics Reports* **336**, 1 (2000).
- ²M. Esposito, U. Harbola, and S. Mukamel, *Reviews of Modern Physics* **81**, 1665 (2009).
- ³L. S. Levitov and G. B. Lesovik, *JETP Lett.* **58**, 230 (1993).
- ⁴L. S. Levitov, H. Lee, and G. B. Lesovik, *Journal of Mathematical Physics* **37**, 4845 (1996).
- ⁵M. Ferrier, T. Arakawa, T. Hata, R. Fujiwara, R. Delagrangé, R. Weil, R. Deblock, R. Sakano, A. Oguri, and K. Kobayashi, *Nature Physics* **12**, 230 (2016).
- ⁶M. Ferrier, T. Arakawa, T. Hata, R. Fujiwara, R. Delagrangé, R. Deblock, Y. Teratani, R. Sakano, A. Oguri, and K. Kobayashi, *Physical Review Letters* **118**, 196803 (2017).
- ⁷R. Vardimon, M. Klionsky, and O. Tal, *Physical Review B* **88**, 161404 (2013).

- ⁸M. Kumar, O. Tal, R. H. M. Smit, A. Smogunov, E. Tosatti, and J. M. van Ruitenbeek, *Physical Review B* **88**, 245431 (2013).
- ⁹R. Vardimon, M. Matt, P. Nielaba, J. C. Cuevas, and O. Tal, *Physical Review B* **93**, 085439 (2016).
- ¹⁰O. S. Lumbroso, L. Simine, A. Nitzan, D. Segal, and O. Tal, *Nature* **562**, 240 (2018).
- ¹¹M. Albert, C. Flindt, and M. Büttiker, *Physical Review Letters* **107**, 086805 (2011).
- ¹²D. S. Kosov, *The Journal of chemical physics* **146**, 074102 (2017).
- ¹³M. Ridley, V. N. Singh, E. Gull, and G. Cohen, *Physical Review B* **97**, 115109 (2018).
- ¹⁴M. Ridley, A. MacKinnon, and L. Kantorovich, *Physical Review B* **95**, 165440 (2017).
- ¹⁵M. Esposito, M. A. Ochoa, and M. Galperin, *Physical Review B* **91**, 115417 (2015).
- ¹⁶S. Nakamura, Y. Yamauchi, M. Hashisaka, K. Chida, K. Kobayashi, T. Ono, R. Leturcq, K. Ensslin, K. Saito, Y. Utsumi, and A. C. Gossard, *Physical Review Letters* **104**, 080602 (2010).
- ¹⁷B. Küng, C. Rössler, M. Beck, M. Marthaler, D. S. Golubev, Y. Utsumi, T. Ihn, and K. Ensslin, *Physical Review X* **2**, 011001 (2012).
- ¹⁸J. P. Pekola, *Nature Physics* **11**, 118 (2015).
- ¹⁹M. Büttiker, *Phys. Rev. Lett.* **57**, 1761 (1986).
- ²⁰A. Croy and U. Saalman, *Physical Review B* **80**, 245311 (2009).
- ²¹G.-M. Tang and J. Wang, *Physical Review B* **90**, 195422 (2014).
- ²²M. Ridley, A. MacKinnon, and L. Kantorovich, *Physical Review B* **91**, 125433 (2015).
- ²³Z. Feng, J. Maciejko, J. Wang, and H. Guo, *Physical Review B* **77**, 075302 (2008).
- ²⁴P.-Y. Yang, C.-Y. Lin, and W.-M. Zhang, *Physical Review B* **89**, 115411 (2014).
- ²⁵T. Zelovich, L. Kronik, and O. Hod, *Journal of Chemical Theory and Computation* **11**, 4861 (2015).
- ²⁶P. Darancet, J. R. Widawsky, H. J. Choi, L. Venkataraman, and J. B. Neaton, *Nano Letters* **12**, 6250 (2012).
- ²⁷L. A. Zotti, T. Kirchner, J.-C. Cuevas, F. Pauly, T. Huhn, E. Scheer, and A. Erbe, *small* **6**, 1529 (2010).
- ²⁸L. Venkataraman, J. E. Klare, W. T. I, C. Nuckolls, M. S. Hybertsen, and M. L. Steigerwald, *Nano Lett.* **6**, 458 (2006).
- ²⁹S. Y. Quek, L. Venkataraman, H. J. Choi, S. G. Louie, M. S. Hybertsen, and J. B. Neaton, *Nano Lett.* **7**, 3477 (2007).
- ³⁰W. Hong, D. Z. Manrique, P. Moreno-García, M. Gulcur, A. Mishchenko, C. J. Lambert, M. R. Bryce, and T. Wandlowski, *Journal of the American Chemical Society* **134**, 2292 (2012).
- ³¹A. Nitzan, *Chemical Dynamics in Condensed Phases: Relaxation, Transfer and Reactions in Condensed Molecular Systems* (Oxford University Press, USA, 2006).
- ³²I. Oz, O. Hod, and A. Nitzan, arXiv:1810.08982 [cond-mat] (2018), arXiv:1810.08982 [cond-mat].
- ³³U. Harbola, M. Esposito, and S. Mukamel, *Physical Review B* **74**, 235309 (2006).
- ³⁴M. Esposito and M. Galperin, *The Journal of Physical Chemistry C* **114**, 20362 (2010).
- ³⁵D. A. Bagrets and Y. V. Nazarov, *Physical Review B* **67**, 085316 (2003).
- ³⁶G. Kießlich, P. Samuelsson, A. Wacker, and E. Schöll, *Physical Review B* **73**, 033312 (2006).
- ³⁷C. Flindt, T. Novotný, A. Braggio, M. Sasseti, and A.-P. Jauho, *Physical Review Letters* **100**, 150601 (2008).
- ³⁸K. Kaasbjerg and W. Belzig, *Physical Review B* **91**, 235413 (2015).
- ³⁹W. Dou, G. Miao, and J. E. Subotnik, *Physical Review Letters* **119**, 046001 (2017).
- ⁴⁰W. Dou, M. A. Ochoa, A. Nitzan, and J. E. Subotnik, *Physical Review B* **98**, 134306 (2018).
- ⁴¹D. N. Zubarev, *Soviet Physics Uspekhi* **3**, 320 (1960).
- ⁴²T. J. Levy and E. Rabani, *The Journal of Chemical Physics* **138**, 164125 (2013).
- ⁴³T. J. Levy and E. Rabani, *Journal of Physics: Condensed Matter* **25**, 115302 (2013).
- ⁴⁴A. Levy, L. Kidon, D. T. Limmer, and E. Rabani, arXiv:1901.04315 [cond-mat, physics:quant-ph] (2019), arXiv:1901.04315 [cond-mat, physics:quant-ph].
- ⁴⁵D. W. H. Swenson, T. Levy, G. Cohen, E. Rabani, and W. H. Miller, *The Journal of Chemical Physics* **134**, 164103 (2011).
- ⁴⁶D. W. Swenson, G. Cohen, and E. Rabani, *Molecular Physics* **110**, 743 (2012).
- ⁴⁷H.-P. Breuer, F. Petruccione, *et al.*, *The theory of open quantum systems* (Oxford University Press on Demand, 2002).
- ⁴⁸M. Esposito and S. Mukamel, *Physical Review E* **73**, 046129 (2006).
- ⁴⁹B. Derrida, *Journal of Statistical Mechanics: Theory and Experiment* **2007**, P07023 (2007).
- ⁵⁰E. Arrigoni, M. Knap, and W. von der Linden, *Physical Review Letters* **110**, 086403 (2013).
- ⁵¹A. Dorda, M. Nuss, W. von der Linden, and E. Arrigoni, *Physical Review B* **89**, 165105 (2014).
- ⁵²A. Dorda, M. Ganahl, H. G. Evertz, W. von der Linden, and E. Arrigoni, *Physical Review B* **92**, 125145 (2015).
- ⁵³F. Chen, G. Cohen, and M. Galperin, *Physical Review Letters* **122**, 186803 (2019).
- ⁵⁴R. Bulla, T. A. Costi, and T. Pruschke, *Reviews of Modern Physics* **80**, 395 (2008).
- ⁵⁵F. B. Anders and A. Schiller, *Physical Review Letters* **95**, 196801 (2005).
- ⁵⁶F. B. Anders, *Journal of Physics: Condensed Matter* **20**, 195216 (2008).
- ⁵⁷F. B. Anders, *Physical Review Letters* **101**, 066804 (2008).
- ⁵⁸M. Pletyukhov and H. Schoeller, *Physical Review Letters* **108**, 260601 (2012).
- ⁵⁹L. G. G. V. Dias da Silva, F. Heidrich-Meisner, A. E. Feiguin, C. A. Büsler, G. B. Martins, E. V. Anda, and E. Dagotto, *Physical Review B* **78**, 195317 (2008).
- ⁶⁰S. Langer, F. Heidrich-Meisner, J. Gemmer, I. P. McCulloch, and U. Schollwöck, *Physical Review B* **79**, 214409 (2009).
- ⁶¹F. Heidrich-Meisner, A. E. Feiguin, and E. Dagotto, *Physical Review B* **79**, 235336 (2009).
- ⁶²F. A. Wolf, I. P. McCulloch, and U. Schollwöck, *Physical Review B* **90**, 235131 (2014).
- ⁶³H. Wang and M. Thoss, *The Journal of Chemical Physics* **119**, 1289 (2003).
- ⁶⁴H. Wang and M. Thoss, *The Journal of chemical physics* **131**, 024114 (2009).
- ⁶⁵E. Y. Wilner, H. Wang, G. Cohen, M. Thoss, and E. Rabani, *Physical Review B* **88**, 045137 (2013).
- ⁶⁶E. Y. Wilner, H. Wang, M. Thoss, and E. Rabani, *Physical Review B* **89**, 205129 (2014).
- ⁶⁷E. Y. Wilner, H. Wang, M. Thoss, and E. Rabani, *Physical Review B* **90**, 115145 (2014).
- ⁶⁸E. Y. Wilner, H. Wang, M. Thoss, and E. Rabani, *Physical Review B* **92**, 195143 (2015).
- ⁶⁹H. Wang and M. Thoss, *Chemical Physics High-Dimensional Quantum Dynamics (on the Occasion of the 70th Birthday of Hans-Dieter Meyer)*, **509**, 13 (2018).
- ⁷⁰F. Schwarz, M. Goldstein, A. Dorda, E. Arrigoni, A. Weichselbaum, and J. von Delft, *Physical Review B* **94**, 155142 (2016).
- ⁷¹D. M. Fugger, A. Dorda, F. Schwarz, J. von Delft, and E. Arrigoni, *New Journal of Physics* **20**, 013030 (2018).
- ⁷²F. Schwarz, I. Weymann, J. von Delft, and A. Weichselbaum, *Physical Review Letters* **121**, 137702 (2018).
- ⁷³Y. Tanimura and P. G. Wolynes, *Physical Review A* **43**, 4131 (1991).
- ⁷⁴J. Jin, X. Zheng, and Y. Yan, *The Journal of Chemical Physics* **128**, 234703 (2008).
- ⁷⁵Z. Li, N. Tong, X. Zheng, D. Hou, J. Wei, J. Hu, and Y. Yan, *Physical Review Letters* **109**, 266403 (2012).

- ⁷⁶R. Härtle, G. Cohen, D. R. Reichman, and A. J. Millis, *Physical Review B* **88**, 235426 (2013).
- ⁷⁷R. Härtle, G. Cohen, D. R. Reichman, and A. J. Millis, *Physical Review B* **92**, 085430 (2015).
- ⁷⁸A. Erpenbeck, C. Hertlein, C. Schinabeck, and M. Thoss, *The Journal of Chemical Physics* **149**, 064106 (2018).
- ⁷⁹Q. Shi, Y. Xu, Y. Yan, and M. Xu, *The Journal of Chemical Physics* **148**, 174102 (2018).
- ⁸⁰N. Makri, *Ann. Rev. Phys. Chem* **50**, 167 (1999).
- ⁸¹D. Segal, A. J. Millis, and D. R. Reichman, *Physical Review B* **82**, 205323 (2010).
- ⁸²L. Simine and D. Segal, *The Journal of Chemical Physics* **138**, 214111 (2013).
- ⁸³S. Weiss, J. Eckel, M. Thorwart, and R. Egger, *Physical Review B* **77**, 195316 (2008).
- ⁸⁴J. Eckel, F. Heidrich-Meisner, S. G. Jakobs, M. Thorwart, M. Pletyukhov, and R. Egger, *New Journal of Physics* **12**, 043042 (2010).
- ⁸⁵M. Kilgour, B. K. Agarwalla, and D. Segal, *The Journal of Chemical Physics* **150**, 084111 (2019).
- ⁸⁶P. Werner, T. Oka, M. Eckstein, and A. J. Millis, *Physical Review B* **81**, 035108 (2010).
- ⁸⁷G. Cohen and E. Rabani, *Physical Review B* **84**, 075150 (2011).
- ⁸⁸G. Cohen, E. Y. Wilner, and E. Rabani, *New Journal of Physics* **15**, 073018 (2013).
- ⁸⁹G. Cohen, E. Gull, D. R. Reichman, A. J. Millis, and E. Rabani, *Physical Review B* **87**, 195108 (2013).
- ⁹⁰E. Gull, A. J. Millis, A. I. Lichtenstein, A. N. Rubtsov, M. Troyer, and P. Werner, *Reviews of Modern Physics* **83**, 349 (2011).
- ⁹¹L. Mühlbacher and E. Rabani, *Physical Review Letters* **100**, 176403 (2008).
- ⁹²M. Schiró and M. Fabrizio, *Physical Review B* **79**, 153302 (2009).
- ⁹³P. Werner, T. Oka, and A. J. Millis, *Physical Review B* **79**, 035320 (2009).
- ⁹⁴M. Schiró, *Physical Review B* **81**, 085126 (2010).
- ⁹⁵E. Gull, D. R. Reichman, and A. J. Millis, *Physical Review B* **84**, 085134 (2011).
- ⁹⁶G. Cohen, E. Gull, D. R. Reichman, and A. J. Millis, *Physical Review Letters* **112**, 146802 (2014).
- ⁹⁷G. Cohen, D. R. Reichman, A. J. Millis, and E. Gull, *Physical Review B* **89**, 115139 (2014).
- ⁹⁸A. E. Antipov, Q. Dong, and E. Gull, *Physical Review Letters* **116**, 036801 (2016).
- ⁹⁹G. Cohen, E. Gull, D. R. Reichman, and A. J. Millis, *Physical Review Letters* **115**, 266802 (2015).
- ¹⁰⁰H.-T. Chen, G. Cohen, and D. R. Reichman, *The Journal of Chemical Physics* **146**, 054105 (2017).
- ¹⁰¹H.-T. Chen, G. Cohen, and D. R. Reichman, *The Journal of Chemical Physics* **146**, 054106 (2017).
- ¹⁰²A. E. Antipov, Q. Dong, J. Kleinhenz, G. Cohen, and E. Gull, *Physical Review B* **95**, 085144 (2017).
- ¹⁰³Q. Dong, I. Krivenko, J. Kleinhenz, A. E. Antipov, G. Cohen, and E. Gull, *Physical Review B* **96**, 155126 (2017).
- ¹⁰⁴A. Boag, E. Gull, and G. Cohen, *Physical Review B* **98**, 115152 (2018).
- ¹⁰⁵R. E. V. Profumo, C. Groth, L. Messio, O. Parcollet, and X. Waintal, *Physical Review B* **91**, 245154 (2015).
- ¹⁰⁶E. A. Polyakov and A. N. Rubtsov, arXiv:1712.04279 [cond-mat] (2017), arXiv:1712.04279 [cond-mat].
- ¹⁰⁷A. Moutenet, P. Seth, M. Ferrero, and O. Parcollet, arXiv:1904.11969 [cond-mat] (2019), arXiv:1904.11969 [cond-mat].
- ¹⁰⁸C. Bertrand, O. Parcollet, A. Maillard, and X. Waintal, arXiv:1903.11636v2 [cond-mat] (2019).
- ¹⁰⁹C. Bertrand, S. Florens, O. Parcollet, and X. Waintal, arXiv:1903.11646 [cond-mat] (2019), arXiv:1903.11646 [cond-mat].
- ¹¹⁰P. Kubiczek, A. N. Rubtsov, and A. I. Lichtenstein, arXiv:1904.12582 [cond-mat] (2019), arXiv:1904.12582 [cond-mat].
- ¹¹¹Z. Cai, J. Lu, and S. Yang, arXiv:1811.08044 [math-ph, physics:physics] (2018), arXiv:1811.08044 [math-ph, physics:physics].
- ¹¹²C. Flindt, T. Novotný, and A.-P. Jauho, *EPL (Europhysics Letters)* **69**, 475 (2004).
- ¹¹³T. Zelovich, L. Kronik, and O. Hod, *Journal of Chemical Theory and Computation* **10**, 2927 (2014).
- ¹¹⁴O. Hod, C. A. Rodríguez-Rosario, T. Zelovich, and T. Frauenheim, *The Journal of Physical Chemistry A* **120**, 3278 (2016).
- ¹¹⁵T. Zelovich, L. Kronik, and O. Hod, *The Journal of Physical Chemistry C* **120**, 15052 (2016).
- ¹¹⁶T. Zelovich, T. Hansen, Z.-F. Liu, J. B. Neaton, L. Kronik, and O. Hod, *The Journal of Chemical Physics* **146**, 092331 (2017).
- ¹¹⁷C. W. Groth, M. Wimmer, A. R. Akhmerov, and X. Waintal, *New Journal of Physics* **16**, 063065 (2014).
- ¹¹⁸A. Weiße, G. Wellein, A. Alvermann, and H. Fehske, *Reviews of Modern Physics* **78**, 275 (2006).
- ¹¹⁹D. Newns, *Phys. Rev.* **178**, 1123 (1969).
- ¹²⁰D. Vollhardt, (1994).
- ¹²¹M. L. Perrin, E. Burzurí, and H. S. van der Zant, *Chemical Society Reviews* **44**, 902 (2015).
- ¹²²L. J. Klein, K. A. Slinker, J. L. Truitt, S. Goswami, K. L. Lewis, S. N. Coppersmith, D. W. van der Weide, M. Friesen, R. H. Blick, D. E. Savage, *et al.*, *Applied Physics Letters* **84**, 4047 (2004).
- ¹²³S. Datta, *Nanotechnology* **15**, S433 (2004).
- ¹²⁴A. C. Hewson, *The Kondo Problem to Heavy Fermions* (Cambridge University Press, Cambridge, 1993).
- ¹²⁵M. Nuss, M. Ganahl, H. G. Evertz, E. Arrigoni, and W. von der Linden, *Physical Review B* **88**, 045132 (2013).
- ¹²⁶R. Landauer, *Nature* **392**, 658 (1998).